Direct imaging of human Rad51 nucleoprotein dynamics on individual DNA molecules

Jovencio Hilario[a,b], Ichiro Amitani[a,b], Ronald J. Baskin[b], and Stephen C. Kowalczykowski[a,b,1]

Departments of [a]Microbiology and [b]Molecular and Cellular Biology, University of California, Davis, CA 95616-8665

This contribution is part of the special series of Inaugural Articles by members of the National Academy of Sciences elected in 2007.

Contributed by Stephen C. Kowalczykowski, November 24, 2008 (sent for review November 8, 2008)

Rad51 protein (Rad51) is central to recombinational repair of double-strand DNA breaks. It polymerizes onto DNA and promotes strand exchange between homologous chromosomes. We visualized the real-time assembly and disassembly of human Rad51 nucleoprotein filaments on double-stranded DNA by single-molecule fluorescence microscopy. Rad51 assembly extends the DNA by ≈65%. Nucleoprotein filament formation occurs via rapid nucleation followed by growth from these nuclei. Growth does not continue indefinitely, however, and nucleoprotein filaments terminate when ≈2 μm in length. The dependence of nascent filament formation on Rad51 concentration suggests that 2–3 Rad51 monomers are involved in nucleation. Rad51 nucleoprotein filaments are stable and remain extended when ATP hydrolysis is prevented; however, when permitted, filaments decrease in length as a result of conversion to ADP-bound nucleoprotein complexes and partial protein dissociation. Dissociation of Rad51 from dsDNA is slow and incomplete, thereby rationalizing the need for other proteins that facilitate disassembly.

nucleation | RecA protein | recombination | self-assembly | single-molecule

Genomes are continually attacked by both endogenous and exogenous agents that damage DNA. DNA damage in the form of DNA breaks can lead to chromosome translocations, cell cycle arrest, and apoptosis. Homologous recombination is an essential biological process that ensures the accurate repair of DNA breaks and thereby contributes to genomic integrity. The recombinational repair of DNA with a break occurs by a multistep process (1–3). The first step requires resection of the broken duplex DNA by a helicase and/or nuclease to produce a region of 3′-terminated single-strand DNA (ssDNA) at the ends of the break (1, 4). These ssDNA tails serve as substrates for the assembly of a DNA strand exchange protein, such as RecA in bacteria or Rad51 in eukaryotes (2, 3, 5). This nucleoprotein filament finds homology in an intact DNA molecule and promotes DNA strand invasion to form an intermediate, termed a joint molecule. Pairing by both processed ends of the broken DNA, and their subsequent replication, results in formation of Holliday junctions. These Holliday junctions undergo branch migration and are resolved enzymatically to produce the repaired DNA.

Rad51 protein (Rad51) assembles on either single- or double-stranded DNA (dsDNA) to produce a nucleoprotein filament that, at saturation, comprises 1 Rad51 monomer for every 3 nucleotides or base-pairs of DNA. Electron microscopy and X-ray crystallography show the Rad51 nucleoprotein filament to be a right-handed helical structure in which the DNA is stretched by ≈50% over its normal B-form length (6, 7). This filament displays ATP hydrolysis activity when assembled on either ssDNA or dsDNA. Rad51 promotes the homologous pairing of ssDNA with dsDNA; however, migration of the nascent DNA heteroduplex is relatively slow. This DNA strand exchange activity is substantially enhanced by RPA, and is regulated by several mediator proteins (Brca2, Rad51 paralogs, Rad52, and Rad54) (3, 4, 8–10).

Although a basic understanding of Rad51 function exists, a more complete description of the concerted molecular events that underlie the homologous pairing process is still unrealized. The dynamics of Rad51 nucleoprotein filament assembly and disassembly, and the interaction between the filament and homologous target DNA, are poorly understood. Although ssDNA is the normal substrate for Rad51-promoted DNA pairing, the interactions of Rad51 with dsDNA are also biologically relevant. Rad51 binds dsDNA with an affinity comparable to that for ssDNA (11). This Rad51-dsDNA complex impedes DNA repair by inhibiting homologous pairing (12). Additionally, as a result of the DNA strand exchange process, Rad51 becomes associated with the newly formed heteroduplex DNA product. If Rad51 is not removed from the heteroduplex DNA, then the ensuing steps of homologous recombination, DNA synthesis and Holliday junction resolution are adversely affected (13).

In this study, we used single-molecule fluorescence microscopy to visualize human Rad51 assembly and disassembly on duplex DNA. Single-molecule methods provide an unparalleled resolution of the real-time dynamics of biological molecules and of biomolecular complexes (see 14–16). Specifically, the application of single-molecule techniques to the study of recombination proteins has revealed aspects of molecular behavior that were not attainable from ensemble methods (17–26). Single-molecule visualization methods have been used to characterize Rad51-nucleoprotein filaments (20, 27); in ref. 27, filament assembly could not be imaged in real time although disassembly could and, in ref. 20, Rad51 filaments were visualized indirectly through competition with a fluorescent dye. Also, magnetic tweezers were used to monitor changes in DNA length due to Rad51 binding in real time, but direct imaging of the assembly process is not possible with this technique (28). Our work complements the previous studies by combining visualization of individual Rad51-DNA complexes and real-time monitoring of their assembly and disassembly.

Here, we directly observe the dynamics of Rad51 nucleoprotein filaments on single dsDNA molecules, using 2 complementary approaches: (*i*) we labeled the end of DNA molecules with a fluorescent tag that allowed real-time monitoring of both the association and dissociation of native Rad51; and (*ii*) we used a fluorescent Rad51 to directly visualize individual nucleoprotein filament nucleation, assembly, and disassembly. We show that Rad51 assembles on DNA by a mechanism that involves frequent nucleation but, unexpectedly, limited filament growth; a finding that reconciles a number of disparate prior conclusions. We show that 2–3 Rad51 monomers are minimally needed to form a stable

Author contributions: J.H., I.A., and S.C.K. designed research; J.H. and I.A. performed research; J.H., I.A., and R.J.B. contributed new reagents/analytic tools; J.H., I.A., and S.C.K. analyzed data; and J.H. and S.C.K. wrote the paper.

The authors declare no conflict of interest.

Freely available online through the PNAS open access option.

[1]To whom correspondence should be addressed. E-mail: sckowalczykowski@ucdavis.edu.

This article contains supporting information online at www.pnas.org/cgi/content/full/0811965106/DCSupplemental.

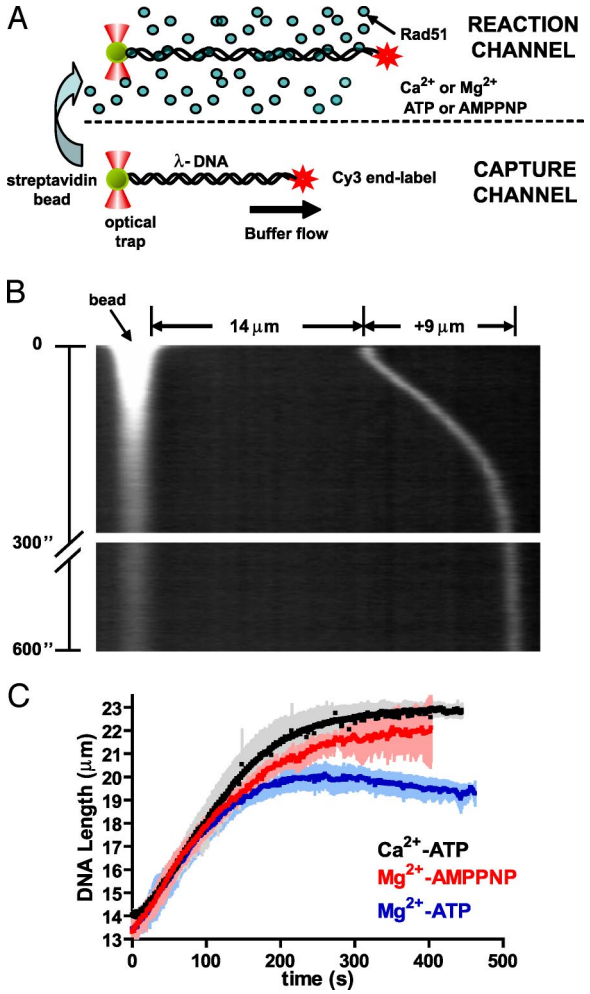

Fig. 1. Assembly of Rad51 protein onto a single molecule of dsDNA measured by extension of Cy3-end-labeled λ DNA. (*A*) Diagram illustrating the assembly of Rad51 onto Cy3, end-labeled λ DNA attached to a bead. Solutions containing DNA-bead complexes (in the capture channel) and Rad51 (in the reaction channel) remain separated because of laminar flow boundaries (indicated by the dashed line). A single end-labeled λ DNA-bead complex is captured in the optical trap and is moved into the reaction channel to allow nucleoprotein filament assembly. (*B*) Kymograph of Rad51 assembly on Cy3-end-labeled λ DNA. The optically trapped bead is on the left side of the kymograph and is fluorescent because of nonspecific Cy3-IgG binding. The unconstrained Cy3-end-label of the λ DNA is on the right side of the kymograph. DNA length is measured from the center of the bead to the Cy3-end label (corrected for the bead radius, $r = 0.5\ \mu m$). Reaction conditions were 100 nM wild-type Rad51, 2 mM $Ca(OAc)_2$, and 1 mM ATP. (*C*) Traces of DNA length versus time for the assembly of Rad51 on DNA in the presence of various cofactors. $Ca(OAc)_2$ and $Mg(OAc)_2$ are at 2 mM, whereas ATP and AMPPNP are at 1 mM.

nucleus. Furthermore, also in contrast to its bacterial homolog, ATP hydrolysis by Rad51 nucleoprotein filaments does not result in rapid dissociation of Rad51 from the dsDNA. This finding rationalizes the need for eukaryotic-specific DNA motor proteins, such as Rad54, that translocate on dsDNA and actively disassemble Rad51 filaments.

Results

Real-Time Visualization of Rad51 Nucleoprotein Filament Assembly Monitored by Extension of DNA Length. To visualize wild-type Rad51 assembly kinetics in real time at the single-molecule level, we used fluorescent end-labeled λ phage DNA (Fig. 1*A*) prepared by separately annealing 3′-biotin and 3′-digoxigenin oligonucleotides to the complementary *cos* sites of λ DNA. The biotinylated end of the DNA was bound to a 1.0 μm streptavidin-coated microsphere to permit capture in an optical laser trap. The opposite end of the λ DNA, with the digoxigenin tag, was reacted first with anti-digoxigenin IgG and then Cy3-labeled anti-IgG secondary antibody to create a fluorescent beacon to monitor the end position of λ DNA by epifluorescence microscopy. This afforded a system whereby different reaction conditions (i.e., protein concentration, divalent metals, and nucleotide cofactors) could be varied and their effects on the rate of native Rad51 assembly could be assessed in real time.

DNA-bead complexes and Rad51 were each introduced into two separate channels of a multichannel flow cell wherein laminar flow prevented mixing of the solutions in the absence of a physical boundary between the channels (21–25, 29). After a single λ DNA-bead complex is captured in the optical trap, it is moved into the reaction channel containing Rad51 (Fig. 1*A*). The position of the Cy3 end-label is determined by 2-dimensional Gaussian fitting of the fluorescence intensity to define the end and, thereby, the length of the DNA. A change in position of the end-label relative to the optically trapped bead is due to DNA extension that accompanies Rad51 binding.

Fig. 1*B* shows a kymograph (a plot of spatial position vs. time) obtained for the real-time assembly of Rad51 (100 nM) on a single λ DNA molecule in the presence of ATP (1 mM) and calcium acetate (2 mM) to prevent ATP hydrolysis (30, 31). At the beginning of the reaction, the λ DNA molecule is ≈14.0 μm in length for the flow rate used. Upon introduction of the DNA-bead complex into the Rad51 reaction channel, there is a short lag phase of ≈10 s, during which the position of the DNA end-label does not change. Afterward, the position of the end-label begins to move away from the bead in the optical trap (toward the right), indicating DNA length extension due to Rad51 binding. After ≈300 s of continuous incubation with Rad51, the DNA is extended by 9.0 μm, which is an apparent 65% increase in length (see also Movie S1). This extension is similar to results obtained for RecA (24) and is slightly greater than seen in structural studies, because of the differences in persistence lengths for duplex DNA and the Rad51 nucleoprotein filament (32).

Human Rad51 was shown to form stable nucleoprotein filaments under conditions of reduced ATP hydrolysis (32); therefore, we examined the Rad51 nucleoprotein assembly in the presence of different divalent metal and nucleotide cofactor partners to assess the effects of ATP hydrolysis. Fig. 1*C* compares the kinetics of DNA extension in the presence Ca^{2+}-ATP, Mg^{2+}-AMPPNP, and Mg^{2+}-ATP. AMPPNP is a nonhydrolyzable ATP analog that can substitute for ATP in DNA strand exchange reactions (32). With limited or no ATP hydrolysis (Ca^{2+}-ATP or Mg^{2+}-AMPPNP), extended nucleoprotein filaments form that are stable and that extend DNA by 64 ± 3% and 63 ± 6%, respectively. In contrast, when ATP hydrolysis occurs (Mg^{2+}-ATP, blue trace), the steady-state nucleoprotein filaments are shorter (DNA extension = 49 ± 3%) because of cycles of Rad51 binding, ATP hydrolysis, Rad51 dissociation, and/or accumulation of ADP-bound Rad51 filaments. Continued observation shows the DNA filaments shorten (by ≈0.6 μm in Fig. 1*C*) from their maximum observed DNA extension of ≈20.0 μm. Shorter filaments were observed in the presence of Mg^{2+}-ATP by single-molecule, total internal reflectance fluorescence microscopy (20) and they correlate with the irregular filaments visualized by scanning force microscopy (32). These experiments establish that by simply measuring DNA length extension, the assembly of Rad51 on single molecules of DNA can be measured in real time; however, such measurements do not permit direct measurement of nucleation and growth.

The Maximum Rate of DNA Length Extension Is Proportional to a Third-Order Dependence on Rad51 Concentration. Recently, single-molecule methods revealed that nucleoprotein filament formation by RecA requires 4–5 monomers to form a nucleus (18, 24) and that

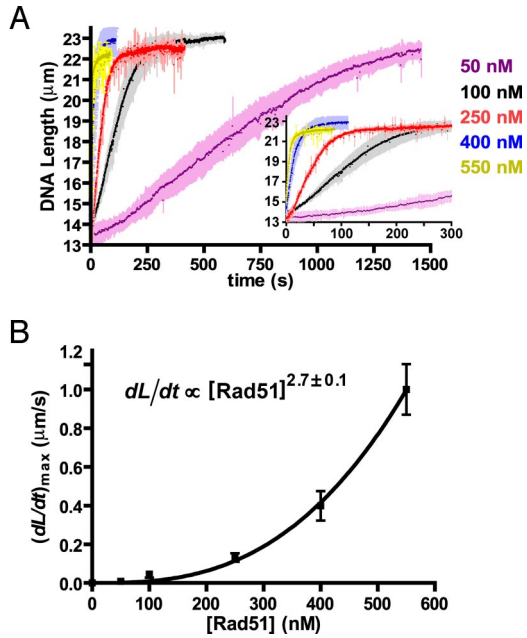

Fig. 2. The rate of Rad51 nucleoprotein formation is sigmoidal in time and follows a third-order dependence on Rad51 concentration. (*A*) Trajectories for DNA length extension due to Rad51 binding as a function of Rad51 concentration. (*Inset*) Expanded view of the initial time course. Each curve represents the mean and standard deviation of 3–4 molecules. Assembly was at 2 mM $Ca(OAc)_2$ and 1 mM ATP. (*B*) Maximum rate of DNA extension versus Rad51 concentration. The maximum rate of DNA extension was obtained from the inflection point of the data in *A*. Solid line is the fit to: $dL/dt = 3 \times 10^{-8}$ [Rad51]$^{2.7}$.

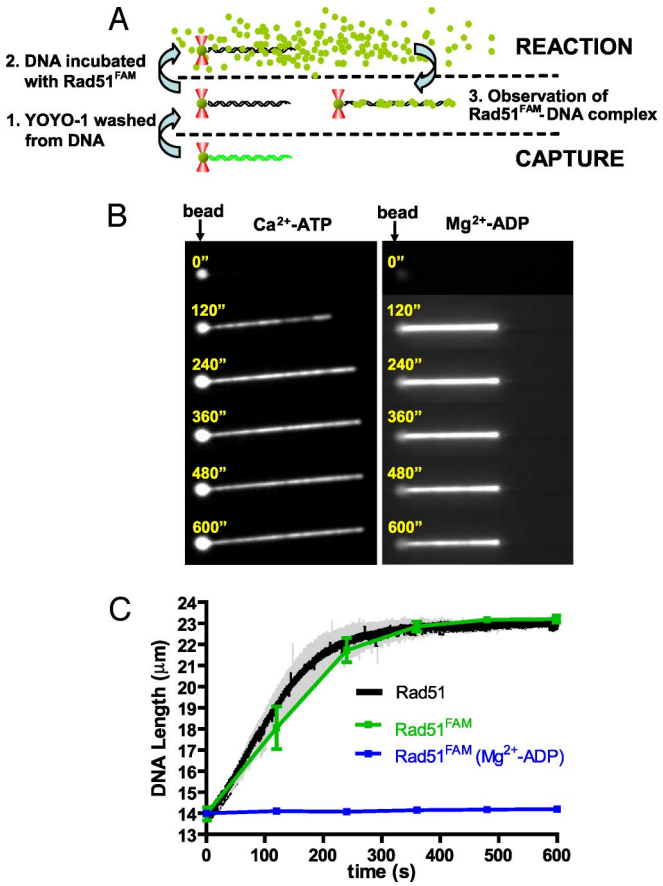

Fig. 3. Fluorescent Rad51 permits direct visualization of nucleoprotein filament formation. (*A*) Diagram of the procedure used to directly image assembly of fluorescent Rad51 onto dsDNA. A 3-channel flow cell is used. A λ DNA-bead complex stained with YOYO-1 is optically trapped in the capture channel. The microscope stage is then translated to move the DNA-bead complex into the middle flow channel to remove bound YOYO-1 (step 1). A second stage movement introduces the DNA-bead complex into the reaction channel (top flow channel) containing fluorescein-labeled Rad51 ($Rad51^{FAM}$) (step 2). Finally, after a specific incubation period, the DNA-bead complex is returned to the middle flow channel to visualize the extent of $Rad51^{FAM}$ binding (step 3). Subsequent incubations with $Rad51^{FAM}$ are performed as necessary. (*B*) Frames from videos (time indicated in seconds) showing $Rad51^{FAM}$ assembly on dsDNA in the presence of Ca^{2+}-ATP (*Left*) and Mg^{2+}-ADP (*Right*). The cumulative incubation times are indicated in each frame. The reactions contained 100 nM $Rad51^{FAM}$, 2 mM $Ca(OAc)_2$, and 1 mM ATP or 500 nM $Rad51^{FAM}$, 2 mM $Mg(OAc)_2$, and 1 mM ADP. (*C*) DNA length extension trajectories for both Rad51 and $Rad51^{FAM}$. Data shown for Rad51 are the same presented in Fig. 2*A*, whereas data for $Rad51^{FAM}$ represent the mean and standard deviation for 4–6 individual DNA molecules; in some cases, the error bars are smaller than the symbols.

elongation occurs by addition of monomers to the existing filament (18). If Rad51 were to behave similarly, then nucleoprotein assembly would occur by 2 elemental steps: (*i*) nucleation: the rate-limiting binding of a stable nucleating species of Rad51 to DNA according to nRad51+DNA $\rightarrow$ $(Rad51)_n$-DNA; and (*ii*) growth: the fast subsequent and potentially indefinite addition of Rad51 monomers to an existing nucleus according to $(Rad51)_n$-DNA + Rad51 $\rightarrow$ $(Rad51)_{n+1}$-DNA. When ATP hydrolysis is limited, the dissociation reactions can be ignored, and only the forward direction of assembly need be considered. These two steps have reaction rates for nucleation and growth that are related to simple power dependencies on Rad51 concentration according to: $rate_n \propto [Rad51]^n$ and $rate_g \propto [Rad51]$, respectively.

The extension of dsDNA versus time is plotted for 5 different Rad51 concentrations spanning 50–550 nM (Fig. 2*A*). All time courses show a sigmoidal trajectory, typical for nucleation and growth processes. At the lowest Rad51 concentration, where the change in DNA length occurs slowly, the initial lag phase is particularly evident and it persists for ≈150 s; complete DNA extension (22.4 ± 0.4 μm; 67 ± 6%) takes ≈25 min. At 100 nM Rad51, a brief lag phase of ≈10 s is detected, but at the higher concentrations, the lag phase is not detectable.

The rates of DNA extension (i.e., the slopes in Fig. 2*A*) also increase in a Rad51 concentration-dependent manner. The maximum rates occur at the inflection point of each trajectory; those rates, as defined by the 1st derivative ($(dL/dt)_{max}$) at the inflection point, are plotted in Fig. 2*B*. If the assembly kinetics in the middle of the Rad51 nucleoprotein filament progress curve are dominated by rapid filament growth through the addition of monomers, as is the case for RecA (18), then the observed rates should vary linearly with Rad51 concentration (step 2 of the kinetic model above). However, for Rad51 we obtain a nonlinear relationship that when fit to a simple power law, $(dL/dt)_{max} = a[Rad51]^n$, yields a value of 2.7 ± 0.1 for n. This approximately third-order dependence of the rate on Rad51 concentration suggests either that nucleoprotein filaments grow by trimer addition, or that filament assembly is dominated by nucleation events involving 2–3 Rad51 monomers with limited growth; this issue will be addressed more fully below, where nucleation is visualized specifically and quantified directly.

Direct Visualization of Fluorescent Rad51 Binding to dsDNA. To visualize Rad51 protein assembly directly, we fluorescently labeled Rad51 protein at the N terminus with 5(6)-carboxyfluorescein (FAM) (24). This fluorescein-labeled Rad51 ($Rad51^{FAM}$) is functional in D-loop formation (*SI Text* and Fig. S1). We directly imaged $Rad51^{FAM}$ nucleoprotein filament formation, using the same methodology that was used to observe RecA nucleoprotein filament formation (24). Fig. 3*A* depicts a schematic of the steps comprising this experiment. Briefly, a single λ DNA-bead complex is trapped

in the capture channel. The DNA is initially stained with the fluorescent dye, YOYO-1, to select beads with only 1 full-length DNA molecule attached. The DNA molecule is then moved to the observation channel (Fig. 3*A*, step 1), where YOYO-1 is dissociated, so as not to affect Rad51 binding. After the YOYO-1 has dissociated, the molecule is transferred to the reaction channel for incubation with $Rad51^{FAM}$ for a selected time interval (Fig. 3*A*, step 2). Finally, the trapped complex is returned to the middle channel for observation (Fig. 3*A*, step 3). Steps 2 and 3 are repeated as necessary for the experiment, and this process will be referred to as "dipping."

Fig. 3*B* shows time-lapsed images of 2 λ DNA molecules that were repeatedly dipped, for the cumulative times indicated, into the $Rad51^{FAM}$ channel at 2 different assembly conditions, Ca^{2+}-ATP (Fig. 3*B Left*) and Mg^{2+}-ADP (Fig. 3*B Right*). At time 0, only the bead is visible because of nonspecific binding of the YOYO-1 dye. In the presence of Ca^{2+}-ATP, a fully extended Rad51-DNA assembles within ≈360 s. When the time course for filament assembly by direct observation of $Rad51^{FAM}$ is compared with the time course obtained by measurement of DNA length extension, using unmodified Rad51 (e.g., as in Fig. 1 and 2), it is evident that the rate of nucleoprotein filament assembly for both proteins is the same (Fig. 3*C*), verifying that the fluorescent modification does not alter the assembly behavior. Interestingly, in the presence of Mg^{2+}-ADP, $Rad51^{FAM}$ does bind dsDNA, resulting in apparent complete coverage of the dsDNA, but elicits only a marginal extension of DNA length (≈1 μm). This is an important finding because it shows that the binding of the ADP-bound form of Rad51 can be overlooked or misinterpreted in single-molecule experiments that measure only DNA length extension.

By using shorter dipping times (20 s), we determined that ATP-Rad51 nucleates along dsDNA at multiple positions (Fig. 4*A*). The image at $t = 0$ shows fluorescence only from the bead. After the first 20 s of incubation with $Rad51^{FAM}$, we see patches of fluorescent Rad51 along much of the length of the DNA molecule. After just 40 s, the DNA contains a high density of partial filaments. We could repeatedly incubate the same DNA-bead complex with $Rad51^{FAM}$ until protein binding and DNA extension were complete (Movie S2). Shorter incubation intervals affected the overall time required to reach a completely extended nucleoprotein filament (compare Fig. 3*B* with Fig. 4*A*), perhaps because of some loss of Rad51 in channel 2; however, longer dipping times (i.e., fewer dips) produced kinetics similar to continuous incubation.

Although we could readily see complete filament formation on single molecules at these assembly conditions, we could not determine whether individual clusters were growing together or whether new nuclei were initiating on naked DNA between clusters. Consequently, we reduced the rate of Rad51 filament assembly, as will be elaborated in the next section, by increasing the solution ionic strength by adding NaCl. The rate of Rad51 nucleation was indeed reduced, and it was now possible to follow the progression of both nucleation and growth of shorter filaments (Fig. 4*B*). One can clearly observe the formation of multiple nucleation clusters, separated by nonfluorescent regions of naked DNA. Yellow arrows in the figure indicate 4 such nucleation clusters (at 18 min), and the magenta arrows point to the first appearance of new nuclei that form adjacent to these existing nuclei (at 30, 42, and 60 min). The isolated nascent clusters are observed to increase in fluorescent intensity and size (up to ≈2 μm) before either new clusters fill in the gap between existing clusters, or 2 filaments appear to unite. Thus, the assembly of Rad51 is seen to occur by nucleation along the entire length of the DNA; however, and in contrast to what is seen for RecA when nucleation is slowed (24), extensive growth does not occur. Instead, complete nucleoprotein filament coverage occurs by the formation of multiple nucleation clusters and their coalescence into apparently continuous filaments (within optical resolution) rather than by extensive filament growth from just a few sites of nucleation.

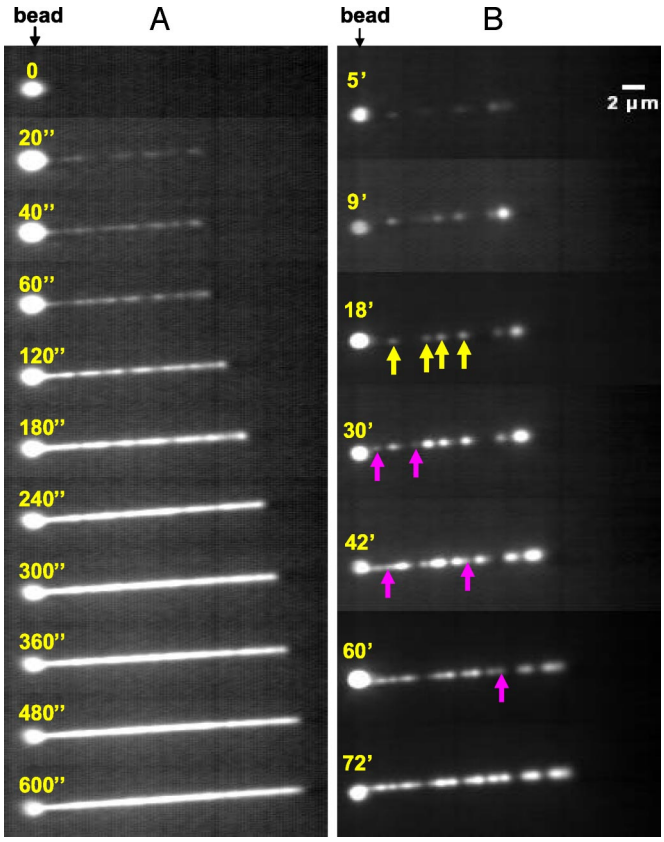

Fig. 4. Rad51 assembles on dsDNA by a process that involves multiple nucleation events followed by limited growth. (*A*) Frames from a video (time indicated in seconds) showing nucleation and growth of $Rad51^{FAM}$ nucleoprotein filament formation on a single λ DNA molecule. The reaction contained 100 nM $Rad51^{FAM}$, 2 mM $Ca(OAc)_2$, and 1 mM ATP. (*B*) Frames from a video (time indicated in minutes) of $Rad51^{FAM}$ assembling on a single λ DNA molecule under suboptimal assembly conditions. The same DNA molecule was repeatedly incubated with 300 nM $Rad51^{FAM}$ in 2 mM $Ca(OAc)_2$, 1 mM ATP, and 200 mM NaCl. Yellow arrows indicate representative nucleation clusters, whereas the magenta arrows mark those nuclei that have newly formed adjacent to an existing cluster. (Scale bar, 2 μm.)

Nucleation of Rad51 Filaments Follows a Third-Order Dependence on Protein Concentration. The use of fluorescent Rad51 allows us to observe nucleation and growth directly. To determine both the nucleation frequency of Rad51 and the minimum number of Rad51 monomers needed to form a stable nucleation site, we examined the Rad51 concentration dependence of cluster formation. However, as indicated above, the rapid binding of Rad51 at low salt concentrations prevented accurate quantification of the nucleation frequency over a useful range of Rad51 concentration. Therefore, we needed to reduce the speed of assembly. The affinity of Rad51 for DNA is reduced by increasing the NaCl concentration (33), and we expected that the assembly process would concomitantly slow. We used this approach to study the nucleation behavior of RecA (24).

Representative images of $Rad51^{FAM}$ assembling on DNA at various elevated NaCl concentrations are presented in Fig. 5*A*. At each NaCl concentration (a vertical strip), a single DNA molecule was repeatedly dipped in the $Rad51^{FAM}$ channel for the times indicated. With increasing NaCl concentration, the nucleation frequency decreases substantially, necessitating a progressively longer dipping time to obtain a reliable number of nuclei. Quantification of the number of clusters formed per unit time confirms that NaCl reduces nucleation frequency (Fig. 5*B*). Control experiments confirmed that the nucleation rates were identical for a single DNA molecule that was repeatedly dipped versus using a

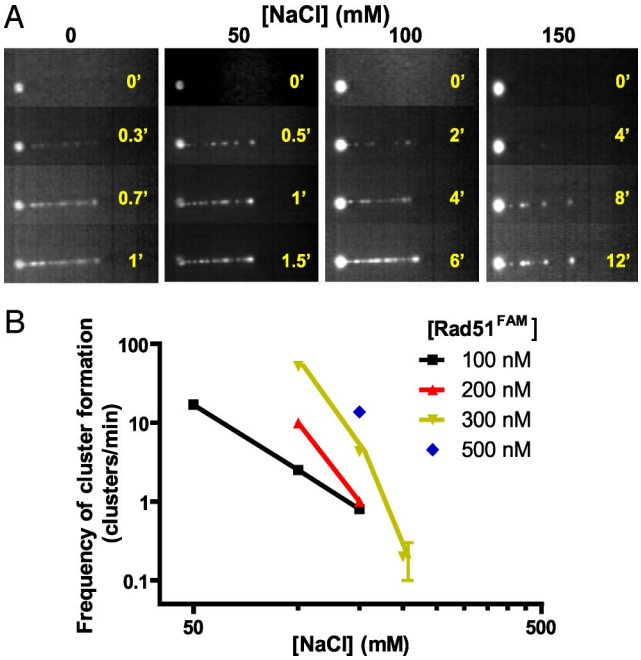

Fig. 5. The rate of Rad51 nucleation on dsDNA is reduced by increasing the solution ionic strength. (*A*) Time-lapsed images of 4 different λ DNA molecules repeatedly incubated with 100 nM Rad51^{FAM} for the indicated times (in minutes) as a function of NaCl concentration. (*B*) Log-log plot of the rate of Rad51^{FAM} nucleation for different protein concentrations as function of NaCl concentration; slopes range from ~−3 to −6. Error bars (most are comparable to, or smaller, than the size of the symbols) are the standard deviation of 4–7 molecules.

different molecule for each time point (data not shown). When these experiments are repeated using a higher concentration of Rad51, the nucleation frequency increases at any given NaCl concentration, offsetting the inhibitory effect of the salt (Fig. 5*B*).

By surveying the effect of NaCl and Rad51 concentration on nucleation frequency, we established that at 150 mM NaCl, it was possible to quantify the nucleation frequency over a wide range of Rad51 concentrations (Fig. 6*A*). Fig. 6*A* shows a single DNA molecule incubated with increasing Rad51 concentrations for the cumulative times. For early dipping times, where the DNA is not overly saturated with Rad51 clusters, quantification shows that formation of nucleation clusters is linear in time (Fig. 6*B*). Nucleation rates range from 0.8 ± 0.1 clusters/min (2.7×10^{-7} s^{-1}·bp^{-1}) at 100 nM Rad51 up to 13.6 ± 0.3 clusters/min (4.7×10^{-6} s^{-1}·bp^{-1}) at 500 nM Rad51. Nucleation rates as a function of Rad51 concentration are presented in Fig. 6*C* and show a nonlinear dependence on protein concentration. The nucleation rate can be fit to a simple power dependence, rate = a[Rad51]^n, as was done for RecA (24). Fitting yields a value of $n = 2.4 \pm 0.2$. This result suggests that ≈3 monomers of Rad51 are required to form a stable nucleus from which filament growth occurs. This third-order dependence on Rad51 concentration was also seen when the maximum rate of DNA extension was quantified (Fig. 2*B*). The implications of this agreement between the different experiments are discussed later. Additionally, this result is comparable with values obtained for RecA, where 4–5 RecA monomers were found to be sufficient for stable cluster formation (18, 24).

Rad51 Disassembly from dsDNA Is Slow and Incomplete. Finally, the disassembly of fully formed Rad51 nucleoprotein filaments was examined both by measuring DNA length (using end-labeled DNA) and by visualizing fluorescein-labeled Rad51 directly. Fig. 7*A* shows kymographs of Rad51 (*Left*) and Rad51^{FAM} (*Right*) nucleoprotein filaments formed using Ca^{2+}-ATP in channel 3 and their real-time disassembly upon introduction to Mg^{2+}-ATP in the observation channel. The length of nucleoprotein filaments, as measured by either the position of the Cy3 end-label or directly for the Rad51^{FAM} nucleoprotein filaments, is seen to decrease slowly. Quantification (Fig. 7*D*) shows that the nucleoprotein filament lengths decrease linearly at rates of 0.0230 ± 0.0004 μm/min (Rad51) and 0.0470 ± 0.0005 μm/min (Rad51^{FAM}). This result

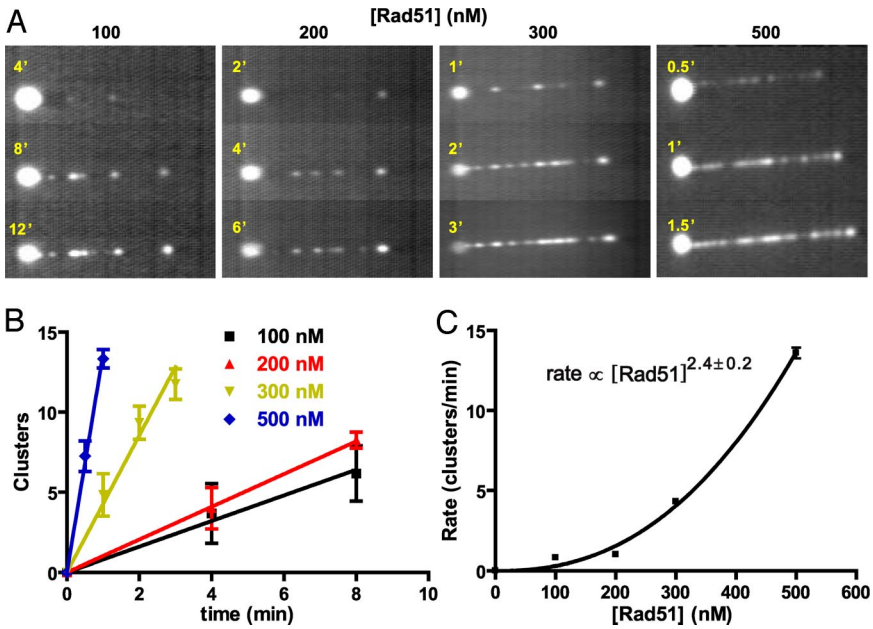

Fig. 6. Approximately 3 Rad51 monomers are required to form a stable nucleus. (*A*) Frames from videos of Rad51^{FAM} nucleation on individual DNA molecules. Each frame shows a single λ DNA molecule incubated repeatedly (cumulative incubation times indicated in minutes) with specified concentrations of Rad51^{FAM}. Reaction conditions are 2 mM $Ca(OAc)_2$, 1 mM ATP, and 150 mM NaCl. (*B*) Time dependence of Rad51^{FAM} cluster formation on dsDNA as a function of Rad51^{FAM} concentration derived from images such as those shown in *A*. Data are the mean and standard deviation of 4–7 individual molecules obtained at each concentration. (*C*) Rate of cluster formation versus Rad51 concentration. Solid line is fit to the expression: rate = 5.2×10^{-6} [Rad51]$^{2.4}$. Standard deviations are the size of the data points.

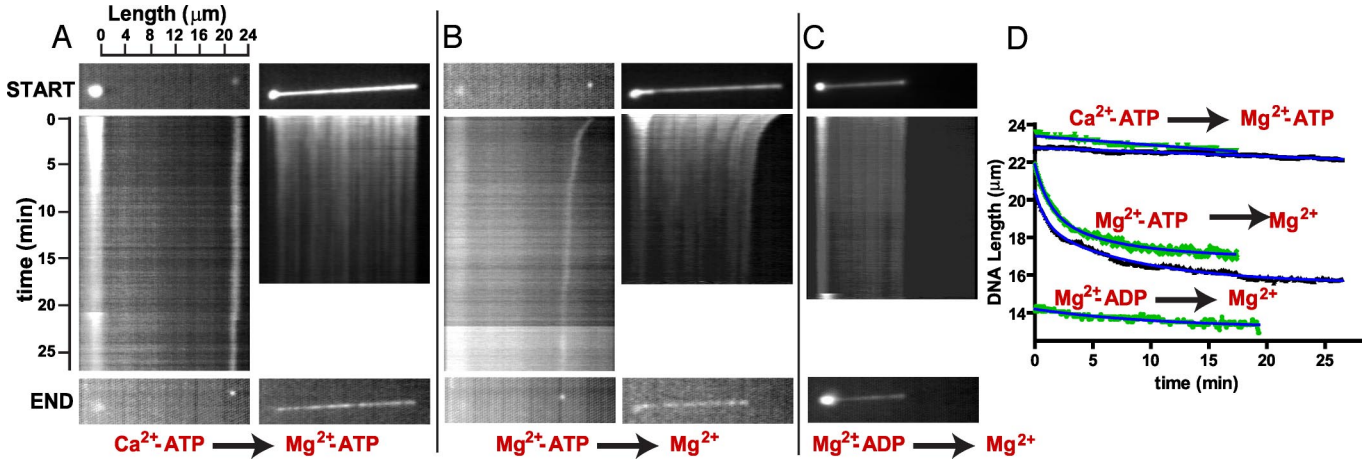

Fig. 7. Rad51 disassembles from dsDNA slowly. (*A*) Rad51 filaments [Rad51 (*Left*) and Rad51^{FAM} (*Right*)] formed in the presence of 2 mM $Ca(OAc)_2$ and 1 mM ATP and allowed to disassemble in the presence of 5 mM $Mg(OAc)_2$ and 2 mM ATP. In *A–C*, still images of the nucleoprotein filaments at the start and end of the reactions are indicated above and below the kymographs. (*B*) Rad51 filaments [Rad51 (*Left*) and Rad51^{FAM} (*Right*)] formed in the presence of 2 mM $Mg(OAc)_2$ and 1 mM ATP and allowed to disassemble in the presence of 5 mM $Mg(OAc)_2$. (*C*) Rad51 filaments (Rad51^{FAM}) formed in the presence of 2 mM Mg^{2+} and 1 mM ADP and allowed to disassemble in the presence of 5 mM Mg^2. The original length of the DNA in this experiment was slightly shorter at ≈13.5 μm and, as such, extended to only ≈14.5 μm. (*D*) Trajectories for the data shown in *A–C*. Experiments using Rad51 are in black; those using Rad51^{FAM} are in green. Solid blue lines represent linear (Ca^{2+}-ATP) and nonlinear (Mg^{2+}-ATP and Mg^{2+}-ADP) fits to the data.

affirms that Rad51 filaments that are prevented from hydrolyzing ATP are stable and do not disassemble. This result differs from a recent report where surface-tethered Rad51 filaments formed in Ca^{2+}-ATP were dissociated upon buffer exchange to Mg^{2+}-ATP (27). This difference in behavior is due to differences in buffer conditions (unpublished data). Furthermore, using bulk phase experiments, we confirmed that Rad51 nucleoprotein filaments preformed with Ca^{2+}-ATP under our conditions do not hydrolyze ATP when Mg^{2+}-ATP is added (data not shown), a finding in agreement with the original observation that Ca^{2+} blocks hydrolysis of Mg^{2+}-ATP by human Rad51 (34) and showing that Mg^{2+}-ATP does not rapidly exchange with the Ca^{2+}-ATP bound to Rad51 nucleoprotein filaments.

In contrast, both Rad51 and Rad51^{FAM} nucleoprotein filaments formed in Mg^{2+}-ATP shorten quickly when moved into an observation channel lacking ATP. (Fig. 7*B Left* and *Right* kymographs). The length of the nucleoprotein filament decreases with an initially rapid phase for the first 150 s; after this rapid decrease, a slower rate of decrease continues. These time courses were best fit to a double exponential decay function (Fig. 7*D*), yielding similar rate constants (both the fast and slow dissociation processes) for both unmodified and fluorescent Rad51 (Rad51: $k_{fast} = 1.00 \pm 0.08\ min^{-1}$, $k_{slow} = 0.11 \pm 0.01\ min^{-1}$; Rad51^{FAM}: $k_{fast} = 0.79 \pm 0.04\ min^{-1}$, $k_{slow} = 0.16 \pm 0.01\ min^{-1}$).

We observed that Rad51 is not completely dissociated from dsDNA up to the maximum experimental times possible. In the case of the end-labeled DNA experiment, dissociation to the point of recovering the original length of the naked DNA (≈14 μm) is not achieved after 25 min. Additionally, in the fluorescent Rad51 experiment, Rad51^{FAM} is still visibly bound over most of the length of the DNA at the end of the experiment, although the fluorescent intensity has greatly diminished because of some dissociation and photobleaching (Fig. 7*B Right* and Movie S3). Fitting of both decay curves (Fig. 7*D*) yielded similar asymptotic values for the final filament length (Rad51 = 15.6 μm, Rad51^{FAM} = 17.0 μm, both ± 0.03 μm)]. Our results above suggested that these stable nucleoprotein filaments are ADP-Rad51-DNA complexes, with possibly some residual ATP bound to monomers within the nucleoprotein filament.

To compare the stability of the post-ATP hydrolysis complex to the ADP-Rad51 complex, nucleoprotein filaments were formed using Mg^{2+}-ADP directly (Fig. 7*C*), and disassembly was triggered by moving the complex into the observation channel lacking ADP (Fig. 7*C*, kymograph). Both the kymograph and the end-point image show that ADP-Rad51 remains bound to DNA for >20 min. The trajectory is also plotted in Fig. 7*D* and gives a disassembly rate of $0.09 \pm 0.005\ min^{-1}$ when fit to a single exponential decay, which is comparable with the value of k_{slow} obtained in the Mg^{2+}-ATP experiments. This result is consistent with our inference that, when starting with an ATP-Rad51 nucleoprotein filament, ATP hydrolysis does not result in immediate dissociation of protein but, rather, in accumulation of an ADP- Rad51 nucleoprotein filament, which is not extended, and that dissociates slowly from the DNA.

Discussion

We have used single-molecule fluorescence microscopy to directly observe the assembly and disassembly of human Rad51 protein onto and from dsDNA. Two approaches were used: measuring the length of fluorescently end-labeled λ DNA and directly visualizing fluorescein-labeled Rad51 protein. The results show that the fluorescent Rad51 behaves identically to the unmodified wild type protein in these single-molecule experiments, and thus, the data obtained from both approaches are complementary.

Visualization of DNA length extension permitted the real-time observation of Rad51 nucleoprotein filament formation. The assembly kinetics are sigmoidal, and the DNA is observed to extend 65% when ATP hydrolysis is prevented. When ATP hydrolysis is permitted, the DNA is extended only 50%, reflecting the dynamic nature of the Rad51 nucleoprotein filaments. The rate of Rad51 nucleoprotein growth, as measured by changes in DNA extension, increases with a third-order dependence on Rad51 concentration. This finding is incongruent with the simplest nucleation and growth model, which posits that growth is indefinite and occurs by addition of Rad51 monomers. However, a resolution of this issue emerged from direct imaging of nucleation and growth. We saw that Rad51 rapidly nucleated along the entire DNA length. However, the new clusters did not grow indefinitely but, instead, grew to a finite length of only ≈2 μm (≈6,000 base pair; because of the spatial resolution of our measurements, these filaments could encompass numerous smaller filament segments). Consequently, complete coverage of the DNA occurred largely by new nucleation events that filled the spaces of naked DNA between the initially sparse clusters. We determined that minimally 2–3 monomers of Rad51 are required to

form a stable nucleus, based on the Rad51 concentration dependence of nucleation.

Finally, we showed that Rad51 nucleoprotein filaments, which are hydrolyzing ATP, shorten by a biexponential process comprising a fast kinetic step followed by a much slower kinetic phase. We attribute the fast step to ATP hydrolysis by Rad51 clusters, and their immediate conversion to the compact ADP-bound nucleoprotein filament. This ADP-Rad51 nucleoprotein filament does not extend DNA appreciably and is unexpectedly stable. Hence, the slower kinetic step most likely represents dissociation of the Rad51-ADP complexes from DNA.

Rad51 Nucleoprotein Filament Formation Occurs by Frequent Nucleation, Involving 2–3 Rad51 Monomers, but Limited Filament Growth. When measured by DNA length extension (Fig. 2), the assembly of Rad51 on dsDNA is sigmoidal with respect to time, displaying a brief lag phase, a rapid extension phase, and a final plateau. For the bacterial homolog, RecA, the lag phase, during which there is little change in DNA length with time, largely represents nucleation of 4–5 monomers, whereas the period of rapid DNA extension represents mostly rapid filament growth through addition of protein monomers to existing nuclei (18, 24). For RecA, filament growth should follow a first-order dependence on protein concentration. However, for Rad51, the observed rates of filament extension are apparently third-order with respect to protein concentration. This finding could imply that growth occurs by addition of trimers to the filament. Such a conclusion would also seem to be in qualitative accord with a recent study that concluded that Rad51 nucleoprotein filaments grow by addition of Rad51 pentamers (28). However, we note that an implicit assumption in the kinetic models is that growth is indefinite: i.e., that once nucleated, a filament can grow to the DNA ends, or until it encounters another filament. In that study, nucleation and growth rates were determined from Monte Carlo fitting of DNA length extension. Both rates followed nearly identical dependences on Rad51 concentration, and yielded Hill coefficients of 4–5; this analysis was interpreted to mean that Rad51 assembled as a pentamer. However, our observations that nucleoprotein filament formation requires repeated nucleation, and that nucleation involves 2–3 Rad51 monomers are sufficient to explain the power dependence of the growth phase: the third-power dependence of nucleation manifests itself in the nucleation-limited DNA length extension measurements. Thus, we conclude that the power dependence of the DNA length extension is a reflection of Rad51 nucleoprotein filament extension occurring by nucleation of many short filaments rather than by rapid growth from a few nuclei. By directly visualizing the appearance of nucleation clusters, we observed that nascent nucleoprotein filaments did not grow indefinitely; instead, DNA coverage required repeated nucleation. A consequence of frequent nucleation, but limited growth, is that many Rad51 nucleoprotein filament segments are produced. They have the potential to unite, if neighboring filaments are in register, but if not, then short gaps of DNA will persist. In this regard, our results agree with those of a recent single-molecule study where a fluorescently modified Rad51 variant was used to visualize nucleoprotein filament formation (27). Fluorescence imaging suggested that nucleation occurred at least once every 2,700 bp, and scanning force microscopy showed that filament segments were ≈500 bp.

The explanation for the failure of Rad51 filaments to grow indefinitely is not clear (28). One possibility is that, even under conditions of limited ATP hydrolysis (i.e., in the presence of calcium and ATP), a small amount of ATP is hydrolyzed to produce an ADP-bound Rad51 species. Conceivably, this ADP-bound species could "cap" or prevent the addition of new monomer to the filament and thereby prevent filament growth. However, when the same experiments were performed in the presence of Mg^{2+} and AMPPNP, multiple nucleation and limited growth was still observed (*SI Text*, Fig. S2, and data not shown). A second possibility is that contaminants in the preparation, such as proteolytic fragments, might be poisoning filament growth. Although difficult to eliminate unambiguously, we used several independent preparations of protein, including one that was repurified on an affinity matrix, ssDNA-cellulose, to remove any inactive protein and the few detectable trace contaminants (*SI Text*, Fig. S3, and data not shown). The behavior of these proteins was identical. A third possibility is that the filaments are capped with a form of Rad51 that cannot support indefinite assembly: such a form could be the closed 6-, 7-, or 8-membered rings that are commonly observed for the RecA/RadA/Rad51/Dmc1 family (35–37) and whose presence inversely correlates with the protein's capacity to promote DNA strand exchange (37). At present, the physical basis for termination of Rad51 nucleoprotein filament size remains to be determined.

Rad51 Disassembly from DNA Is Slow, Revealing the Need for a Catalyst. We can observe that dissociation of Rad51 from dsDNA is slow. We conclude that the reduction in filament length involves conversion of ATP-bound Rad51 to the compact ADP-bound form, which accumulates on DNA, and that this species has an unexpected long half-life of ≈5 (±1) minutes (Fig. 7*D*). Furthermore, we saw that ADP-Rad51 binds along the entire length of the DNA, but that these filaments are barely extended. Electron microscopy showed that human Rad51 nucleoprotein filaments in the presence of ATP are extended (≈150%) and active, which is similar to the active form of RecA nucleoprotein filaments. However, the inactive Rad51 nucleoprotein filaments, which were formed after incubation (15 min) with ATP, were condensed and resembled the ADP-RecA nucleoprotein filament (38). This comparison, when taken with the recent finding that human Rad51-ATP filaments on ssDNA are quickly converted to an inactivated ADP-bound form that is slow to release ADP (34), supports our observations and conclusions.

A consequence of having inactivated Rad51 filaments bound relatively stably to heteroduplex DNA is that the steps of recombinational DNA repair subsequent to DNA strand invasion would be hindered. This consideration explains the requirement for a catalyst, Rad54, to accelerate dissociation of Rad51 from dsDNA. Rad51 needs to be cleared from the heteroduplex DNA product formed during DNA strand invasion, and this task is performed by the translocating DNA motor protein, Rad54 (25, 39–41). Furthermore, because of its high affinity for dsDNA, in vivo observations confirm that Rad51 and its homologs associate with undamaged chromosomes to form dead-end complexes (42). In the case of the Rad51 homolog, Dmc1, these nonproductive chromosomal complexes are disassembled by Tid1, a Rad54 homolog (26, 42, 43). Disassembly of Rad51 nucleoprotein filaments occurs by association of Rad54 with the end of a nucleoprotein filament segment and suggests that Rad54 may target ADP-Rad51 nucleoprotein filaments (41); hence, the fact that Rad51-dsDNA filaments being relatively short and discontinuous both permits and promotes Rad54-mediated disassembly. Thus, our single-molecule approaches have revealed unexpected features of Rad51 nucleoprotein filament assembly and disassembly that are compatible with, and explain, the function of other components of the cellular machinery. They reveal that the behavior of individual nucleoprotein filaments of Rad51 [and RecA (24)] resembles mechanistically the self-assembly of systems such as actin and tubulin (44, 45), including nucleation requiring multiple protomers; end-biased bidirectional growth; growth capping; filament stability determined by liganded state; modulation of stability by NTP hydrolysis; and control of both nucleation and growth—one notable difference, however, is the need for a DNA template to mediate the self-assembly (46). It should be possible to use our imaging methods to study more complex aspects of these reactions in real time without the limitations of traditional ensemble methods.

Materials and Methods

Single-Molecule Fluorescence Microscopy. All experiments were performed using an epifluorescence microscope equipped with an optical laser trap as reported in refs. 21, 22, 24, 25. A 3-channel flow-cell was used for all experiments. Single-molecule buffer (SMB) consisted of 50 mM TrisOAc (pH 8.0), 15% sucrose, and 30 mM DTT and was degassed and filtered (0.2 μm) before use. The reaction temperature was 28 °C, and the flow rate was 50 μL/h (linear flow rate $\approx$200 μm/s).

For the experiments with fluorescent end-labeled DNA, single DNA molecules were captured in the first channel of the flow-cell and moved to the second channel by translating the microscope stage. The second channel contained the indicated concentrations of Rad51, either 2 mM $Ca(OAc)_2$ or $Mg(OAc)_2$, and either 1 mM ATP or AMPPNP (Sigma). The third channel was used to monitor association or dissociation, and contained SMB, plus the indicated components. All steps were continually visualized in real time.

Single-molecule imaging of fluorescent Rad51 nucleoprotein filament formation and dissociation was performed as follows. First, DNA-bead complexes were captured using the laser trap. The DNA-bead complexes were stained with YOYO-1dye (10 nM final) to visualize the starting length of the DNA molecule. The YOYO-1-DNA-bead complex was moved laterally to the second channel containing SMB and either 5 mM $Ca(OAc)_2$ or $Mg(OAc)_2$. This step removes the intercalated YOYO-1 to prevent interference with Rad51 binding. DNA-bead complex was moved to the third channel and was incubated with fluorescent Rad51 in SMB containing either 2 mM $Ca(OAc)_2$ or $Mg(OAc)_2$ with 1 mM nucleotide cofactor (ATP, AMPPNP, or ADP) for the specified times, after which the protein-DNA-bead complex was brought back to the second channel for direct observation. All data were collected on S-VHS tape, digitized and analyzed with ImageJ (version 1.33u). All linear and nonlinear regression analyses were performed using Prism software (version 4.0 or 5.0, GraphPad).

ACKNOWLEDGMENTS. We thank Wolf-Dietrich Heyer and members of the S.C.K. laboratory (Jason Bell, Aura Carreira, Petr Cejka, Clarke Conant, Christopher Dombrowski, Anthony Forget, Taeho Kim, Edgar Valencia-Morales, Katsumi Morimatsu, Amitabh Nimonkar, Jody Plank, Behzad Rad, Liang Wang, and Jason Wong) for their thorough reading of the manuscript and Andrzej Stasiak for suggesting that filaments might be capped with rings. This work was supported by National Institutes of Health Grant GM-64745 (to S.C.K.) and Susan G. Komen Postdoctoral Fellowship PDF0707927 (to J.H.).

1. Spies M, Kowalczykowski SC (2005) Homologous recombination by RecBCD and RecF pathways. *The Bacterial Chromosome*, ed Higgins NP (Am Soc Microbiol, Washington, DC).
2. Kuzminov A (1999) Recombinational repair of DNA damage in *Escherichia coli* and bacteriophage λ. *Microbiol Mol Biol Rev* 63:751–813.
3. Pâques F, Haber JE (1999) Multiple pathways of recombination induced by double-strand breaks in Saccharomyces cerevisiae. *Microbiol Mol Biol Rev* 63:349–404.
4. Symington LS (2002) Role of RAD52 epistasis group genes in homologous recombination and double-strand break repair. *Microbiol Mol Biol Rev* 66:630–670.
5. Bianco PR, Tracy RB, Kowalczykowski SC (1998) DNA strand exchange proteins: A biochemical and physical comparison. *Front Biosci* 3:D570–D603.
6. Ogawa T, Yu X, Shinohara A, Egelman EH (1993) Similarity of the yeast RAD51 filament to the bacterial RecA filament. *Science* 259:1896–1899.
7. Conway AB, *et al.* (2004) Crystal structure of a Rad51 filament. *Nat Struct Mol Biol* 11:791–796.
8. Sung P, Klein H (2006) Mechanism of homologous recombination: Mediators and helicases take on regulatory functions. *Nat Rev Mol Cell Biol* 7:739–750.
9. West SC (2003) Molecular views of recombination proteins and their control. *Nat Rev Mol Cell Biol* 4:435–445.
10. Heyer WD, Li X, Rolfsmeier M, Zhang XP (2006) Rad54: The Swiss Army knife of homologous recombination? *Nucleic Acids Res* 34:4115–4125.
11. Benson FE, Stasiak A, West SC (1994) Purification and characterization of the human Rad51 protein, an analogue of E. coli RecA. *EMBO J* 13:5764–5771.
12. Sung P, Robberson DL (1995) DNA strand exchange mediated by a RAD51-ssDNA nucleoprotein filament with polarity opposite to that of RecA. *Cell* 82:453–461.
13. Solinger JA, Kiianitsa K, Heyer WD (2002) Rad54, a Swi2/Snf2-like recombinational repair protein, disassembles Rad51:dsDNA filaments. *Mol Cell* 10:1175–1188.
14. Bustamante C, Chemla YR, Forde NR, Izhaky D (2004) Mechanical processes in biochemistry. *Annu Rev Biochem* 73:705–748.
15. Charvin G, Strick TR, Bensimon D, Croquette V (2005) Tracking topoisomerase activity at the single-molecule level. *Annu Rev Biophys Biomol Struct* 34:201–219.
16. Rasnik I, Myong S, Ha T (2006) Unraveling helicase mechanisms one molecule at a time. *Nucleic Acids Res* 34:4225–4231.
17. Fulconis R, Mine J, Bancaud A, Dutreix M, Viovy JL (2006) Mechanism of RecA-mediated homologous recombination revisited by single molecule nanomanipulation. *EMBO J* 25:4293–4304.
18. Joo C, *et al.* (2006) Real-time observation of RecA filament dynamics with single monomer resolution. *Cell* 126:515–527.
19. Mameren J, *et al.* (2006) Dissecting elastic heterogeneity along DNA molecules coated partly with Rad51 using concurrent fluorescence microscopy and optical tweezers. *Biophys J* 91:L78–L80.
20. Prasad TK, Yeykal CC, Greene EC (2006) Visualizing the assembly of human Rad51 filaments on double-stranded DNA. *J Mol Biol* 363:713–728.
21. Bianco PR, *et al.* (2001) Processive translocation and DNA unwinding by individual RecBCD enzyme molecules. *Nature* 409:374–378.
22. Spies M, *et al.* (2003) A molecular throttle: The recombination hotspot χ controls DNA translocation by the RecBCD helicase. *Cell* 114:647–654.
23. Handa N, Bianco PR, Baskin RJ, Kowalczykowski SC (2005) Direct visualization of RecBCD movement reveals cotranslocation of the RecD motor after χ recognition. *Mol Cell* 17:745–750.
24. Galletto R, Amitani I, Baskin RJ, Kowalczykowski SC (2006) Direct observation of individual RecA filaments assembling on single DNA molecules. *Nature* 443:875–878.
25. Amitani I, Baskin RJ, Kowalczykowski SC (2006) Visualization of Rad54, a chromatin remodeling protein, translocating on single DNA molecules. *Mol Cell* 23:143–148.
26. Nimonkar AV, Amitani I, Baskin RJ, Kowalczykowski SC (2007) Single molecule imaging of Tid1/Rdh54, a Rad54 homolog that translocates on duplex DNA and can disrupt joint molecules. *J Biol Chem* 282:30776–30784.
27. Modesti M, *et al.* (2007) Fluorescent human RAD51 reveals multiple nucleation sites and filament segments tightly associated along a single DNA molecule. *Structure* 15:599–609.
28. van der Heijden T, *et al.* (2007) Real-time assembly and disassembly of human RAD51 filaments on individual DNA molecules. *Nucleic Acids Res* 35:5646–5657.
29. Spies M, Amitani I, Baskin RJ, Kowalczykowski SC (2007) RecBCD enzyme switches lead motor subunits in response to χ recognition. *Cell* 131:694–705.
30. Mazina OM, Mazin AV (2004) Human Rad54 protein stimulates DNA strand exchange activity of hRad51 protein in the presence of Ca^{2+}. *J Biol Chem* 279:52042–52051.
31. Menetski JP, Varghese A, Kowalczykowski SC (1988) Properties of the high-affinity single-stranded DNA binding state of the Escherichia coli recA protein. *Biochemistry* 27:1205–1212.
32. Ristic D, *et al.* (2005) Human Rad51 filaments on double- and single-stranded DNA: Correlating regular and irregular forms with recombination function. *Nucleic Acids Res* 33:3292–3302.
33. Zaitseva EM, Zaitsev EN, Kowalczykowski SC (1999) The DNA binding properties of Saccharomyces cerevisiae Rad51 protein. *J Biol Chem* 274:2907–2915.
34. Bugreev DV, Mazin AV (2004) Ca^{2+} activates human homologous recombination protein Rad51 by modulating its ATPase activity. *Proc Natl Acad Sci USA* 101:9988–9993.
35. Passy SI, *et al.* (1999) Human Dmc1 protein binds DNA as an octameric ring. *Proc Natl Acad Sci USA* 96:10684–10688.
36. McIlwraith MJ, *et al.* (2001) RadA protein from Archaeoglobus fulgidus forms rings, nucleoprotein filaments and catalyses homologous recombination. *Nucleic Acids Res* 29:4509–4517.
37. Yang S, Yu X, Seitz EM, Kowalczykowski SC, Egelman EH (2001) Archaeal RadA protein binds DNA as both helical filaments and octameric rings. *J Mol Biol* 314:1077–1085.
38. Liu Y, *et al.* (2004) Conformational changes modulate the activity of human RAD51 protein. *J Mol Biol* 337:817–827.
39. Bugreev DV, Mazina OM, Mazin AV (2006) Rad54 protein promotes branch migration of Holliday junctions. *Nature* 442:590–593.
40. Solinger JA, Lutz G, Sugiyama T, Kowalczykowski SC, Heyer WD (2001) Rad54 protein stimulates heteroduplex DNA formation in the synaptic phase of DNA strand exchange via specific interactions with the presynaptic Rad51 nucleoprotein filament. *J Mol Biol* 307:1207–1221.
41. Kiianitsa K, Solinger JA, Heyer WD (2006) Terminal association of Rad54 protein with the Rad51-dsDNA filament. *Proc Natl Acad Sci USA* 103:9767–9772.
42. Symington LS, Heyer WD (2006) Some disassembly required: Role of DNA translocases in the disruption of recombination intermediates and dead-end complexes. *Genes Dev* 20:2479–2486.
43. Holzen TM, Shah PP, Olivares HA, Bishop DK (2006) Tid1/Rdh54 promotes dissociation of Dmc1 from nonrecombinogenic sites on meiotic chromatin. *Genes Dev* 20:2593–2604.
44. Frieden C (1985) Actin and tubulin polymerization: The use of kinetic methods to determine mechanism. *Annu Rev Biophys Bioengr Chem* 14:189–210.
45. Desai A, Mitchison TJ (1997) Microtubule polymerization dynamics. *Annu Rev Cell Dev Biol* 13:83–117.
46. Kowalczykowski SC (1991) Biochemistry of genetic recombination: Energetics and mechanism of DNA strand exchange. *Annu Rev Biophys Biophys Chem* 20:539–575.